Covalent Adduction of Human Serum Albumin by 4-Hydroxy-2-Nonenal: Kinetic Analysis of Competing Alkylation Reactions†

Matthew E. Szapacs,‡ James N. Riggins,‡ Lisa J. Zimmerman,‡,§ and Daniel C. Liebler*,‡,§

Department of Biochemistry and Mass Spectrometry Research Center, Vanderbilt University School of Medicine, Nashville, Tennessee 37232-0146

Received March 16, 2006; Revised Manuscript Received July 11, 2006

ABSTRACT: The electrophilic lipid oxidation product 4-hydroxy-2-nonenal (HNE) reacts with proteins to form covalent adducts, and this damage has been implicated in pathologies associated with oxidative stress. HNE adduction of blood proteins, such as human serum albumin (HSA), yields adducts that may serve as markers of oxidative stress in vivo. We used liquid chromatography−tandem mass spectrometry (LC-MS-MS) and the P-Mod algorithm to map the sites of 10 adducts formed by reaction of HNE with HSA in vitro. The detected adducts included Michael adducts formed at histidine and lysine residues. The selectivity of HNE in competing adduction reactions was evaluated by analysis of kinetics for HNE Michael adduction at six targeted HSA histidine residues. Reaction kinetics were analyzed by selected reaction monitoring in LC-MS-MS using stable isotope tagging with phenyl isocyanate. Rate constants ranged over 4 orders of magnitude, with the order of reactivity being H242 > H510 > H67 > H367 > H247 ≈ K233. The most reactive target, H242, is located in a fatty acid- and drug binding cavity in subdomain IIa of HSA and appears to be a hot-spot for HNE modification. Analysis of adduction kinetics together with HSA structure and target residue pK_a values suggest that location in the hydrophobic binding cavity and low predicted pK_a of H242 account for its high reactivity toward HNE. H242 adducts may be preferred products of adduction by lipophilic electrophiles and may comprise a family of biomarkers for oxidative stress.

The formation of oxidants is a hallmark of chemical toxicity, inflammation, and other types of environmental stresses (*1*, *2*). Oxidative stress and oxidants also are involved in human diseases that account for significant morbidity and mortality, including cancer, atherosclerosis, neurodegenerative diseases, metabolic syndrome, and type 2 diabetes (*3*−*9*). Although oxidative stress derives fundamentally from the excessive flux of reduced oxygen species, such as superoxide, hydrogen peroxide and hydroxyl radicals, secondary products of lipid, DNA and protein oxidation may play critical roles in oxidant-associated molecular pathologies. Lipid peroxidation yields a variety of electrophilic, nonradical products, such as malondialdehyde, hydroxyalkenals, oxoalkenals, epoxyalkenals, and γ-ketoaldehydes (*10*, *11*). 4-hydroxy-2-nonenal (HNE),[1] generated from the oxidation of ω-6 polyunsaturated fatty acids, is a prototypical lipid peroxidation product that modifies protein nucleophiles by both 1,4-addition (Michael addition) and 1,2-addition (Schiff base formation) to the α,β-unsaturated carbonyl system (*12*−*17*). HNE has been shown to be neurotoxic (*18*), to induce apoptosis (*19*, *20*), to cause changes in global gene expression (*21*), and to inactivate several enzymes through modification of nucleophilic amino acid residues (*22*−*24*). In addition, anti-HNE immunoreactivity has been found in tissue from patients with Alzheimer's disease (*25*, *26*), chronic alcoholic liver disease (*27*), atherosclerosis (*28*, *29*), and diabetes (*30*). These observations indicate that HNE protein modifications are characteristic of pathologies associated with oxidative stress that is thought to underlie many diseases.

A major barrier to effective clinical evaluation of oxidative stress is a paucity of good biomarkers, despite years of work in this area. Isoprostane products of lipid oxidation are considered "gold standard" biomarkers for the assessment of systemic oxidative stress and have been extensively validated in animal and human studies (*31*, *32*). A recent comparison of several different biomarkers in rodent models of oxidative stress indicated that only plasma isoprostanes and plasma protein-bound malondialdehyde equivalents accurately reflected the course of oxidative stress in vivo (*33*). The nature of the protein aldehyde adducts measured was not clarified, but these probably include adducts to abundant serum proteins, such as albumin.

Human serum albumin (HSA) is a 66-kDa protein necessary for colloidial stability of blood. HSA plays a major role in bioavailability of drugs, is well-known to carry various

† This work was supported by National Institutes of Health Grants DK071304, ES010056, and ES000267.

* To whom correspondence should be addressed. Phone: 615-322-3063. Fax: 615-343-8372. E-mail: daniel.liebler@vanderbilt.edu.

‡ Department of Biochemistry.

§ Mass Spectrometry Research Center.

[1] Abbreviations: HNE, 4-hydroxy-2-nonenal; HSA, human serum albumin; LC-MS-MS, liquid chomatography−tandem mass spectrometry; MS-MS, tandem mass spectrometry; PBS, phosphate-buffered saline (pH 7.2), containing 1.54 mM potassium phosphate monobasic, 2.71 mM sodium phosphate dibasic, 155.17 mM sodium chloride; PIC, phenylisocyanate; TBS, Tris-buffered saline, containing 10 mM Tris base (pH 7.5), 100 mM sodium chloride; TBST, Tris-buffered saline with Tween, containing 10 mM Tris Base (pH 7.5), 100 mM sodium chloride, 0.1% Tween 20; TCEP, tris(carboxyethyl)phosphine.

10.1021/bi060535q CCC: $33.50
Published on Web 08/15/2006

lipophilic molecules through the circulatory system (*34*, *35*), and is an attractive target for biomarker studies because it is highly abundant, constituting over half of total serum protein (*36*). HSA contains numerous nucleophilic residues that react with electrophiles (*37*−*40*) and is easily isolated from plasma and serum by affinity capture with hydrophobic dyes (*41*) or antibodies (*42*). Because the lifetime of HSA in plasma is approximately 3 weeks, damage to HSA is indicative of relatively recent events in vivo (*34*).

The application of MS-MS together with new data analysis algorithms provides powerful tools for sequence specific analysis of protein adducts, and we have used this approach to map a number of different covalent adducts on proteins (*16*, *43*−*47*). However, a key issue in evaluating specific protein adducts as candidate biomarkers is the relative reactivity of different protein nucleophilic sites with electrophiles, which ultimately dictates the levels of different adducts. We recently described an N-terminal stable isotope tagging method to quantify specific protein adducts in LC-MS-MS of tryptic digests of modified proteins (*48*). Here we have adapted this LC-MS-MS approach to discover potential biomarkers of oxidative stress as HNE adducts on HSA and to characterize the kinetics of these competing adduction reactions. We identified several histidine and lysine residues as sites for the adduction of HSA by HNE in vitro. Application of stable isotope tagging for relative quantitation of the adducts allowed us to compare rates for modification of the different residues simultaneously. Evaluation of kinetic reactivity in the context of HSA structure suggests that both noncovalent complexation of the electrophile with specific protein sites and basicity of nucleophile targets govern reaction rates. These factors may enable predictions of "hot spots" for protein adduction and the identities of candidate biomarkers for oxidative stress.

EXPERIMENTAL PROCEDURES

Reagents. HSA, iodoacetamide, and phenylisocyanate (PIC) were purchased from Sigma-Aldrich (St. Louis, MO). [$^{13}C_6$]-PIC (99%) was purchased from Isotech (Miamisburg, OH). HNE was obtained from Cayman Chemical (Ann Arbor, MI). A monoclonal mouse antibody to the HNE Michael adduct was purchased from Oxis Research (Portland, OR). Tris(carboxyethyl)phosphine (TCEP) was from Pierce (Rockford, IL) and modified porcine sequencing grade trypsin was obtained from Promega (Madison, WI). Serum samples collected from normal human donors were collected as part of an IRB-approved study and were provided by Dr. W. G. Yarbrough, Vanderbilt University School of Medicine.

Purification of HSA from Human Serum. HSA was purified from human serum by affinity chromatography with HiTrap Blue HP columns (1 mL, Amersham Biosciences, Piscataway, NJ). Serum (100 μL) was loaded onto a column preequilibrated with PBS, pH 7.2 at a flow rate of 0.3 mL min^{-1}. After loading of the sample, the column was washed for 15 min, and then bound protein was eluted isocratically with PBS (pH 7.2) containing 2 M NaCl over 35 min. The A_{280} peak containing HSA eluted between 16 and 20 min in a volume of approximately 1.5 mL. The eluent buffer was removed by centrifugation though 10 000 molecular weight cutoff spin filters (Millipore). The retained HSA on the filter was then washed twice with 1 mL of 2 M NaCl prior to use. SDS−PAGE analysis indicated that the purified HSA displays comparable purity to commercially purchased (Sigma) HSA (Supporting Information Figure 1).

Modification of HSA with HNE. HSA was dissolved in PBS (pH 7.2) to 5 μM and treated with 3.2 mM HNE for up to 24 h at room temperature. The reactions then were quenched and labile adducts were stabilized by reduction of HNE carbonyls or Schiff base imines with 100 mM $NaBH_4$ for 15 min at room temperature and then frozen at −20 °C, while the remaining samples were collected. The samples then were thawed, and the buffer was removed by ultrafiltration through 10 000 molecular weight cutoff spin filters and the reduced, adducted HSA was resuspended in 0.1 M ammonium bicarbonate.

Western Blot Analysis of HNE-Adducted HSA. HSA (Sigma) was treated with HNE as described above, except that the reaction samples were frozen at −20 °C to stop the reactions, and the adducts were not reduced with $NaBH_4$ (this was done because the antibody used was raised against the unreduced HNE adduct). HNE-modified HSA was resolved by SDS−PAGE on a 10% NuPAGE Novex Bis-Tris gel (Invitrogen, Carlsbad, CA) and transferred onto a PVDF gel-blotting membrane (Invitrogen). The membranes were blocked with 1:1 mixture of blocking buffer for near-infrared fluorescent Western blotting (Rockland, Gilbertsville, PA) and TBS. The membrane was then incubated with a primary mouse antibody directed toward the histidine-Michael adduct of HNE (Oxis Research) at a 1:500 antibody dilution in 1:1 blocking buffer/TBST solution overnight at 4 °C and washed three times with TBST. The membrane then was incubated with an Alexafluor 680-conjugated goat anti-mouse secondary antibody (Molecular Probes/Invitrogen) (1:5000 antibody dilution in 1:1 blocking buffer/TBST) for 2 h at room temperature and again washed three times with TBST. The membrane was imaged using the LI-COR Odyssey imaging system (LI-COR, Lincoln, NE).

Sample Digestion and Preparation for LC-MS-MS Analysis. HNE-adducted, $NaBH_4$-treated HSA samples were dissolved in 0.1 M ammonium bicarbonate and disulfides were reduced with 4 mM TCEP for 30 min at 50 °C followed by alkylation of cysteine thiols with 20 mM iodoacetamide at room temperature in the dark for 30 min. The reduced, alkylated HSA samples were digested with modified sequencing grade trypsin in a 1:50 trypsin/protein ratio for 16 h at 37 °C. Digestions were stopped with 2% (v/v) (2 μL) formic acid and then either labeled with PIC (see below) or diluted to 1 μg mL^{-1} in 0.1% (v/v) aqueous formic acid for LC-MS-MS analysis.

PIC Labeling of Modified Peptides. PIC labeling was carried out as previously described with slight modifications (*48*). For N-terminal peptide labeling, digested HSA peptides were diluted to approximately 0.05 mg mL^{-1} in 0.1 M ammonium bicarbonate, pH 8 and treated with 10 mM PIC-[$^{12}C_6$] (light label) or PIC-[$^{13}C_6$] (heavy label) for 30 min at 37 °C. The reaction was terminated by adding formic acid to a final concentration of 2% (v/v).

For kinetic analyses of HSA adduction, samples corresponding to all time points were labeled with the light ($^{12}C_6$)-PIC, and a separate sample from the 24 h time point was labeled with the heavy ($^{13}C_6$)-PIC. The light PIC labeled samples each were mixed with an amount of the 24 h PIC-[$^{13}C_6$] labeled sample corresponding to an equal amount of

HSA protein and then diluted to approximately 1 μg mL^{-1} in 0.1% (v/v) formic acid for analysis by LC-MS-MS. For the time points used (0, 30 min, 2, 6, 12, 18, and 24 h), this yielded seven samples for analysis (0 h light/24 h heavy, 30 min light/24 h heavy, 2 h light/24 h heavy, 6 h light/24 h heavy, 12 h light/24 h heavy, 18 h light/24 h heavy, 24 h light/24 h heavy).

LC-MS-MS Analysis, Adduct Identification, and Quantitation. LC-MS-MS analyses were performed on a Thermo LTQ linear ion trap instrument (Thermo Electron, San Jose, CA) equipped with a Thermo Surveyor HPLC system and microautosampler. Peptides were resolved on a 100 μm $\times$ 11 cm fused silica capillary column (Polymicro Technologies, LLC., Phoenix, AZ) packed with 5 μm, 300 Å Jupiter C18 (Phenomenex, Torrance, CA). Liquid chomatography was carried out at ambient temperature at a flow rate of 0.6 μL min^{-1} using a gradient mixture of 0.1% (v/v) formic acid in water (solvent A) and 0.1% (v/v) formic acid in acetonitrile (solvent B). Peptides eluting from the capillary tip were introduced into the LTQ source in microelectrospray mode with a capillary voltage of approximately 2 kV. For adduct identification analyses, a full scan was obtained for eluting peptides in the range of 350−2000 amu followed by four data-dependent MS-MS scans. MS-MS spectra were recorded using dynamic exclusion of previously analyzed precursors for 30 s with a repeat of 1 and a repeat duration of 2. MS-MS spectra are generated by collision induced dissociation of the peptide ions at peptide bonds to generate a series of b- and y-ions as major fragments. The b ions contain the N-terminus of the original peptide ion, whereas the y ions contain the C-terminus (*49*). MS-MS data were evaluated using the Sequest algorithm to determine protein coverage, and spectra corresponding to HNE adducts were identified using P-Mod (*47*). Detection of modified or variant sequences is based on the fact that any modifications of the primary peptide sequence will result in a shift in the peptide mass as well as a shift in the values of any b- and/or y ions that contain the modification. Mass shifts of 158 corresponded to $NaBH_4$-reduced Michael adducts, and mass shifts of 140 corresponded to $NaBH_4$-reduced Schiff base adducts.

Kinetic analysis of HNE adduction at individual HSA amino acid targets was done with the same LC-MS-MS instrumentation, except that the LTQ was set up to perform one full scan (350−2000 amu) followed by MS-MS scans for the specific *m*/*z* values of the doubly or triply charged, HNE adducted, [$^{12}C_6$] and [$^{13}C_6$] PIC-labeled peptides (see Supporting Information, Table 1 for targeted *m*/*z* values). Thermo Xcalibur software was used to extract selected ion chromatograms corresponding to three b- or y-ions characteristic of each PIC-labeled peptide adduct precursor. Integration of the corresponding peaks was carried out for light and heavy PIC-labeled peptide ion pairs, and then the three light/heavy peak ratios for each target peptide were averaged to yield an overall light/heavy ratio for each peptide adduct at each time point. Values of k_{obs} were taken from plots of light/heavy peptide adduct ratios versus time. This analysis was carried out 2−5 times for each peptide adduct.

RESULTS

Identification of HNE Adduction Sites on HSA in Vitro. Preliminary experiments to establish electrophile alkylation conditions used Western blotting to detect HNE Michael adducts on HSA histidine residues. Commercially purchased (Sigma) HSA was incubated with 3.2 mM HNE in PBS buffer for up to 24 h, and samples then were probed for immunoreactivity with a primary mouse antibody directed toward the HNE-Michael adduct (Figure 1). Maximal adduction occurred at the 6 h time point, with little change observed between 6 and 24 h.

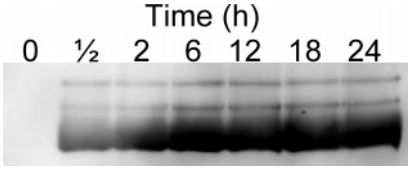

FIGURE 1: Western blot analysis of HNE adduction on HSA. HSA 5 μM was incubated in PBS with 3.2 mM HNE, and aliquots were removed at 0, 30 min, 2, 6, 12, 18, and 24 h. HNE-histidine Michael adducts were detected with mouse anti-HNE primary antibody.

Table 1: HNE Adduct Formation on Sigma HSA and HSA Freshly Purified from Serum[a]

peptide sequence[b]	residue no.	Sigma 24 h	purified 24 h
LVNEVTEFAK*TCVAD	K51	1/5[c]	ND[d]
SLH*TLFGDK	H67	5/5	5/5
NECFLQH*K	H105	1/5	ND
AEFAEVSK*LVTDLTK	K233	3/5	3/5
VH*TECCHGDLLECADDR	H242	3/5	2/5
VHTECCH*GDLLECADDR	H247	1/5	ND
ADLAK*YICENQDSISSK	K262	ND	1/5
CCAAADPH*ECYAK	H367	3/5	ND
VFDEFK*PLVEEPQNLIK	K378	1/5	2/5
EFNAETFTFH*ADICTLSEK	H510	ND	1/5

[a] Commercially purchased (Sigma) HSA and freshly purified HSA were incubated with 5 mM HNE for 24 h and HNE adducts were detected by LC-MS-MS analysis as described under Experimental Procedures. [b] Asterisk (*) indicates adducted residue. [c] Indicates number of times the HNE-adducted peptide was detected in five separate experiments. [d] ND, HNE-adducted peptide not detected.

HNE adduction sites on HSA were identified by LC-MS-MS on both commercially purchased (Sigma) HSA and HSA freshly purified from human serum after 24 h exposure to HNE. Data from five independent experiments for each HSA preparation are summarized in Table 1. (MS-MS spectra of all of the adducts are presented as Supporting Information, Figures 1−10.) A total of 10 adduct sites were identified, including K51, H67, H105, K233, H242, H247, K262, H367, K378 and H510. All of the adducts detected were identified as +158 Da mass shifts with P-Mod, which correspond to $NaBH_4$-reduced Michael adducts. Although Schiff base adducts of HNE were not detected, these adducts would have been detectable had they been present. In other preliminary studies using similar incubation conditions and analytical methods, both Michael and Schiff base adducts of acrolein and crotonaldehyde were detected (data not shown).

Four adducts (K51, H67, K262, and H510) were detected in only one experiment, suggesting that these adducted peptides were either present in low abundance or did not ionize sufficiently well to be reproducibly detected. The H105 adduct was found in one experiment only with the commercial HSA, whereas the other adducts were found repeatedly in multiple experiments in both the commercially purchased HSA and the freshly purified HSA.

Kinetics of HNE Adduction on HSA in Vitro. The ten His and Lys residues targeted by HNE all occupy different

reaction environments that would affect their susceptibility to adduction. To better probe these differences, we sought to simultaneously measure rate constants (k_{obs} values) for adduction at different HSA targets. These measurements would establish the heirarchical reactivity of HSA targets toward HNE. Because we were concerned that differences between the Sigma HSA and the purified HSA preparation could affect adduction kinetics, we performed these analyses with both preparations.

The most straightforward approach would be absolute quantitation of each of the adducted peptides using stable isotope labeled internal standards (*50*). However, this approach requires the synthesis and purification of isotope-labeled peptides containing the adducts of interest, which would be time-consuming and expensive.

Instead, we applied a stable isotope tagging strategy for relative quantitation we described previously (*48*). The approach applies light and heavy isotope tags and LC-MS-MS to compare the amount of an adduct at a given time point to the amount of the same adduct in a reference sample. In our experiments, HSA was treated with HNE, and samples were taken at several time points (0, 30 min, 2, 6, 12, 18, and 24 h). Each sample was treated with $NaBH_4$ to reduce and stabilize the HNE adducts, the protein was then digested with trypsin, and the peptides were N-terminally labeled with light ($^{12}C_6$) PIC. The reference sample was another aliquot of the 24 h sample, which was processed identically, except that the tryptic peptides were tagged with the heavy ($^{13}C_6$) PIC. An aliquot of light PIC-labeled sample for each time point then was mixed in a 1:1 ratio (based on HSA protein) with an aliquot of the heavy PIC-tagged reference sample, and each sample pair was analyzed by LC-MS-MS.

LC-MS-MS analyses on the LTQ targeted *m*/*z* values for the doubly and/or triply charged ions corresponding to the light and heavy PIC-labeled peptides for the 10 adducted HSA peptides. Quantitation was achieved by plotting selected ion chromatograms for three different product ions arising from fragmentation of each targeted precursor. (The *m*/*z* values targeted for MS-MS analysis for light and heavy PIC-labeled forms of the 10 peptide adducts and the corresponding product ion *m*/*z* values are provided as Supporting Information, Table 1). Integrated peak areas for each selected product ion were used-to-calculate ratios for light/heavy PIC-labeled peptide adducts. The ratios calculated from the three different product ions for each peptide adduct then were averaged, and the average value was plotted against the corresponding reaction time. After plotting the light/heavy ratio for each of the time points, a one phase exponential association nonlinear regression analysis was done using Prism graph (Figure 2). Of the 10 peptides that were identified as possible adduction sites, we were able to acquire satisfactory kinetic data on six of these peptide adducts (H67, K233, H242, H247, H367, and H510) and the doubly adducted H242/H247 peptide in both the commercially purchased HSA and the purified HSA. (Relatively low intensity signals were observed for the other adducts, which precluded accurate estimates of peak areas and area ratios.) This allowed the calculation of k_{obs} values for each of the adducted HSA residues (Table 2). Using this approach, we were able to determine the relative reaction rates to be H242 > H510 > H67 > H367 > H247 > K233 for the commercially available HSA and H242 > H510 > H67 > H367 > K233 > H247 for the purified HSA.

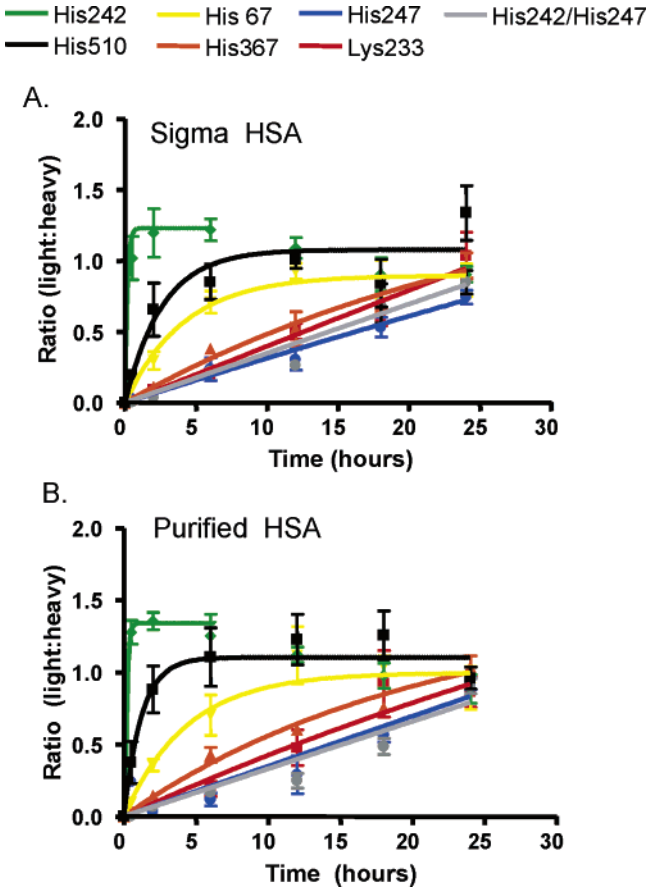

FIGURE 2: (A,B) Kinetic analysis of HNE adduction on HSA. HNE-treated samples were analyzed by LC-MS-MS and stable isotope tagging of peptide adduct N-termini with light and heavy PIC as described in Experimental Procedures.

DISCUSSION

The formation of aldehyde adducts on proteins in vivo may yield biomarkers of oxidative stress and oxidant-related disease. Adducts on HSA are of particular interest because HSA is an abundant blood protein that binds many endogenous and exogenous substances. Covalent modifications of HSA byproducts of lipid peroxidation could offer useful biomarkers of oxidative stress. Our use of LC-MS-MS provided a means to map sites of HSA adduction by HNE and analyze the kinetics of these modification reactions. HSA sites with high reactivity toward HNE in vitro are likely sites of modification in vivo and thus candidate biomarkers for oxidative stress.

We identified 10 sites of HNE modification on HSA. Each of these 10 sites was found to be modified by +158 amu indicating formation of the Michael adduct, whereas no evidence of Schiff base adducts (+140 amu) was found in this experiment. This is in agreement with a recent study by Sayre et al., which reported spectroscopic observation of HNE Michael adducts with lysine side chains on ribonuclease A and β-lactoglobulin, but no evidence for Schiff base formation (*18*). These data indicate that, if it occurs, Schiff base formation by HNE in vitro is considerably slower than Michael adduction.

Table 2: Measured Values of k_{obs} for HNE Adduction and Estimated pK_a Values for the Target Amino Acids[a]

peptide sequence	amino acid	k_{obs} (h^{-1}) (Sigma HSA)	k_{obs} (h^{-1}) (purified HSA)	calculated pK_a
VH*TECCHGDLLECADDR[b]	H242	3.7 ± 0.6[c]	7.9 ± 3.8[c]	0.81
EFNAETFTFH*ADICTLSEK	H510	0.38 ± 0.07	0.81 ± 0.13	7.15
SLH*TLFGDK	H67	0.24 ± 0.02	0.23 ± 0.03	7.65
CCAAADPH*ECYAK	H367	0.035 ± 0.008	0.049 ± 0.006	6.85
VHTECCH*GDLLECADDR	H247	0.006 ± 0.009	0.0008 ± 0.01	8.64
AEFAEVSK*LVTDLTK	K233	0.0013 ± 0.01	0.016 ± 0.01	10.29
VH*TECCH*GDLLECADDR	H242/H247	0.0012 ± 0.01	0.0005 ± 0.011	ND

[a] Values for k_{obs} ± SEM were measured by isotope tagging and LC-MS-MS as described under Experimental Procedures. Values for pK_a were estimated with the PropKa tool (http://propka.chem.uiowa.edu/). See text for discussion. [b] Asterisk (*) indicates adducted residue. [c] These k_{obs} values were calculated from nonlinear regressions fit to data excluding the 12, 18, and 24 h time points.

We were able to evaluate reaction kinetics for only six of the 10 sites identified to be HNE adducted. Of the sites that we were unable to evaluate, three (H105, K51 and K262) were only identified in one experiment in either the Sigma HSA or purified HSA sample, and one (K378) was found in at least one experiment in the Sigma HSA as well as the purified HSA. Our inability to obtain satisfactory kinetic data on these peptide adducts is most likely due to low rates of adduction of these residues that yielded adduct levels near the limit of detection or poor ionization of these peptide adducts. With the exception of H510, the six peptide adducts for which we obtained kinetic data were found in multiple experiments at multiple time points using both the commercially available HSA or the purified HSA and thus were either relatively abundant or ionized particularly well by electrospray. Suppression of ionization by the N-terminal PIC modification used for quantitation is unlikely, as PIC modification did not suppress ionization of the other adducts we observed.

The reaction rates of HNE for both the Sigma HSA and the purified HSA indicated a similar heirarchy of reactivities in both preparations. However, the k_{obs} for H247 was ~10-fold greater in the Sigma HSA than in the purified HSA, whereas K233 had a k_{obs} ~10-fold greater in the purified HSA preparation than in the Sigma HSA. We attribute these discrepancies to the higher experimental error in measurement of slower reactions, which were still in the linear portion of curve after a 24 h time course (e.g., H247, K233 and H242/247). Although the purities of the two HSA preparations studied appeared comparable, we recognize that other proteins may affect measured rate constants by interacting with HSA binding sites. If this occurred, it evidently did not affect the relative reactivities of competing nucleophilic sites.

The reactivities of the different adduction sites varied considerably, as the measured k_{obs}values ranged over more than 4 orders of magnitude. The most reactive site in both HSA preparations was H242, followed by H510, H67, H367, H247, and K233 in order of decreasing reactivity. The tryptic peptide VHTECCHGDLLECADDR containing both H242 and H247 was particularly interesting. These two His residues were the most and (nearly) least reactive, respectively, in HSA yet are separated by only five residues positions in linear sequence. Analysis of the reaction kinetics of H242 revealed that levels of this adduct peaked at 2−6 h of HNE exposure and then declined (Figure 2). Use of selected ion monitoring to search for the doubly adducted H242/H247 peptide indicated formation of the doubly adducted peptide at a slightly slower rate than for the singly H247 adducted peptide.

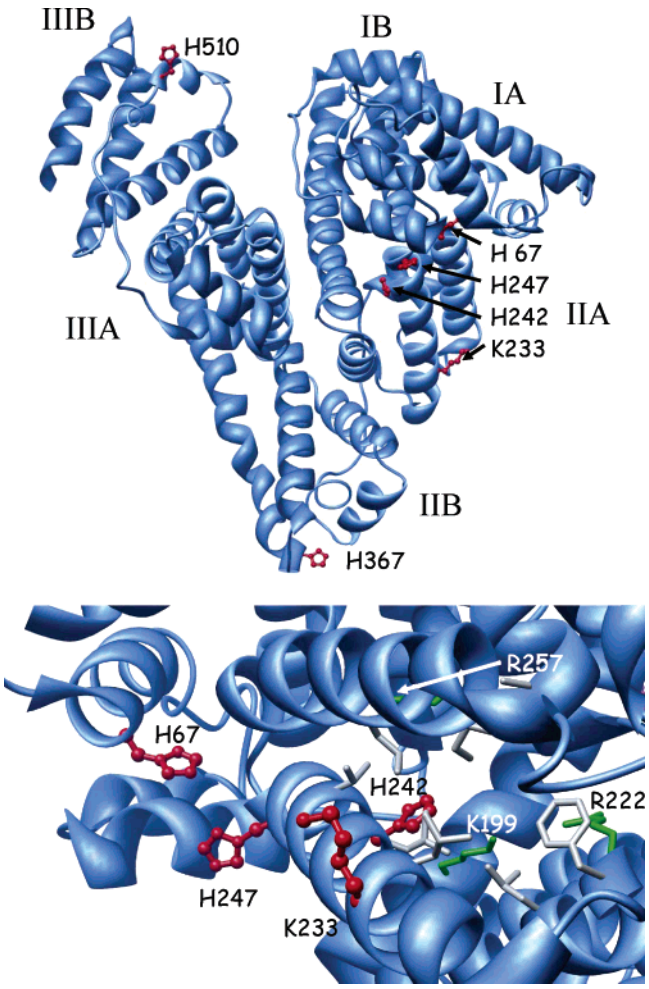

FIGURE 3: HSA crystal structure (PDB: 1AO6) with adducted residues shown in red (top). HSA subdomain IIA with kinetically analyzed adducted residues is shown in red, nonpolar residues in the IIA binding pocket are shown in gray, and the K199, R222, and R257 are shown in green (bottom).

The structures of native HSA and HSA complexes with several small molecule ligands have been reported, and these provide a useful framework for interpreting differences in site-specific HNE adduction. We can use this information to ask how differences in reaction rate may be influenced by structural environments of the adducted residues. Of the targets for which kinetic reactivity was evaluated, H67 is located in subdomain IA, K233, H242, and H247 are located in subdomain IIA, H367 is located in subdomain IIB, and H510 is located in subdomain IIIB of the HSA protein (Figure 3A). Interestingly, the majority of the adduction sites were located in subdomain IIA, which is known to be a fatty

acid/drug binding site (*51*). K233 and H247 are located on the solvent accessible face of subdomain IIA with H67 located on subdomain IA pointing toward the solvent accessible surface of subdomain IIA. In contrast, H242, the most reactive residue, lies in the interior of this subdomain (Figure 3B) in a cavity lined with the hydrophobic residues L219, F223, L234, L238, V241, L260, A261, I264, I290, and A291 (Figure 3B, shown in gray) and with the positively charged K199, R222, and R257 residues (Figure 3B shown in green).

HSA has been cocrystallized with several saturated (*52*, *53*) and unsaturated fatty acids (*54*), as well as with small molecules such as triiodobenzoic acid (*51*), the hormone thyroxine (*55*), and the anticoagulant warfarin (*56*), and this IIA subdomain cavity was shown to bind all of these molecules. The hydrophobic cavity in subdomain IIA accommodates the hydrophobic chains of the fatty acids or the aromatic rings of the small molecules and the polar carboxylic acid or ketone groups are ion paired with K199, R222, or R257. If the nonpolar tail of HNE sits similarly in this cavity and the aldehyde and the 4-hydroxy group of HNE can hydrogen bond with K199, R222, or R257, then H242 is positioned to form the 1,4-Michael adduct with HNE. This analysis suggests that noncovalent complexation of the electrophile with a protein target can be a powerful directing factor in site-specific protein alkylation.

Another potentially important factor in site reactivity is the nucleophilicity and basicity of the target residue. We used PROPKA, an algorithm that estimates pK_a values for amino acid side chains in proteins from their crystal structures (*57*). We submitted the HSA Protein Data Bank file 1AO6 to the PROPKA server (http://propka.chem.uiowa.edu/) for analysis of the pK_a values for His and Lys residues in HSA using the PDB2PQR (*58*) tool to add hydrogen atoms and optimize the hydrogen bonding network at pH 7. This analysis indicated that because of desolvation effects and its ability to ion pair with K199, H242 had the lowest pK_a in the HSA structure, followed in order of increasing pK_a by H367, H510, H67, H247, K233 (Table 2). The trend in the estimated pK_a values correlates with measured k_{obs} values, thus suggesting that lower basicity (lower pK_a) favors the deprotonated target and more rapid adduction by HNE. The unusually low estimated value for the H242 pK_a lends support to our finding that H242 is the most reactive residue toward HNE. We can attribute the high reactivity of H242 not only to favorable juxtaposition of HNE with the H242 imidazole through noncovalent complexation but also to the very low pK_a value of the target, which increases the effective concentration of the deprotonated nucleophile.

We observed that H67 reacted faster with HNE than H247, even though both residues are located within 4 Å of each other. Nevertheless, the H67 pK_a is estimated to be one unit lower than that for H247. Thus, an HNE molecule in proximity to both H67 and H247 will react preferentially at H67 because of its lower pK_a. In addition, the adducted H67 may then block adduction at H247 because, once formed, the HNE adduct on H67 may sterically hinder access to H247, thus making H247 one of the slowest reacting residues in HSA.

Except for H367, the other residues follow the trend that as pK_a increases, HNE reactivity decreases. Interestingly, while both H367 and H510 are on the solvent accessible surface and H367 has a slightly lower pK_a, H510 is the second most reactive residue, whereas H367 is the fourth most reactive residue. Examination of the structures reveals that H367 sits down in a cleft in the HSA molecule, whereas H510 protrudes into the solvent (Figure 4). This indicates that the HNE molecule may encounter steric hindrance when reacting with H367, whereas H510 is more accessible for reaction with HNE.

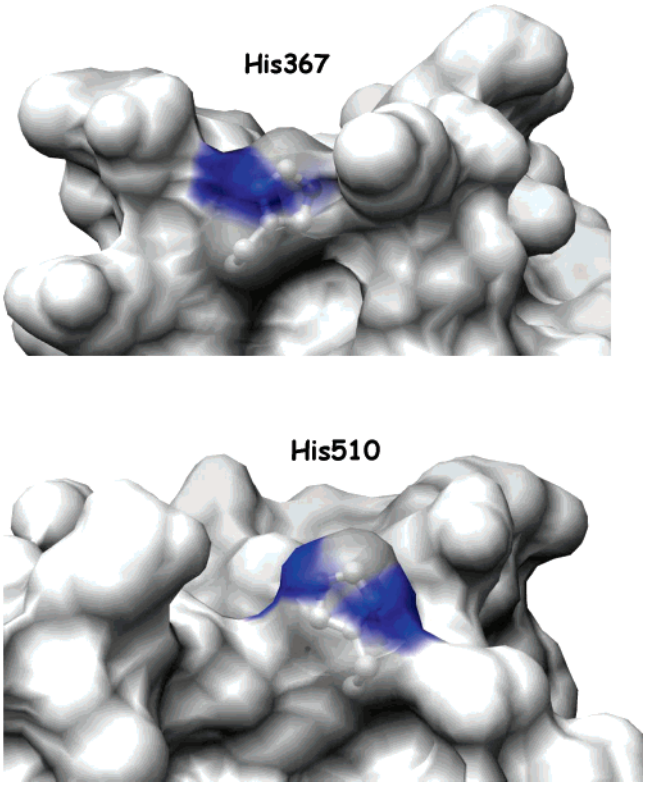

FIGURE 4: Crystal structure of HSA (PDB: 1AO6) with His367 (A) and His510 (B) highlighted surfaces.

Our adduct mapping and the kinetic analyses of HSA adduction by HNE reveal that protein targeting by electrophiles is a complex process. Site selectivity for protein adduction derives from the rate constants for multiple competing adduction reactions. Each of these rate constants in turn is dependent on the basicity and nucleophilicity of individual nucleophilic residues, as well as their steric accessibility. Moreover, the extremely high reactivity of H242 suggests that noncovalent complexation of the electrophile can drive reactivity by favorably orienting the electrophile toward the nucleophile target.

Finally, the observation that H242 is highly reactive toward HNE is significant because modification of this residue may readily occur when HSA is exposed to HNE or structurally similar electrophiles under conditions of oxidative stress. Thus, targeted analyses directed at this peptide may detect biomarkers of oxidative stress in vivo. HSA adducts thus may complement recently identified ascorbyl-HNE adducts (*59*) as new biomarkers of oxidative stress.

ACKNOWLEDGMENT

We thank Prof. Jens Meiler, Prof. Charles Sanders, and Dr. Eric Dawson for helpful discussion on structural biology and pK_a calculations.

SUPPORTING INFORMATION AVAILABLE

SDS−PAGE analyses of both purified and Sigma HSA and the MS-MS spectra of the 10 identified HNE adducted peptides and a table of the targeted *m*/*z* values used to monitor for the light and heavy PIC labeled HNE adducted peptides. This material is available free of charge via the Internet at http://pubs.acs.org.

REFERENCES

1. Ames, B. N. (1983) Dietary carcinogens and anticarcinogens. Oxygen radicals and degenerative diseases, *Science 221*, 1256−1264.
2. Halliwell, B. (1994) Free radicals, antioxidants, and human disease: curiosity, cause, or consequence? *Lancet 344*, 721−724.
3. Butterfield, D. A. (2002) Amyloid beta-peptide (1−42)-induced oxidative stress and neurotoxicity: implications for neurodegeneration in Alzheimer's disease brain. A review, *Free Radic. Res. 36*, 1307−1313.
4. Perry, G., Nunomura, A., Hirai, K., Zhu, X., Perez, M., Avila, J., Castellani, R. J., Atwood, C. S., Aliev, G., Sayre, L. M., Takeda, A., and Smith, M. A. (2002) Is oxidative damage the fundamental pathogenic mechanism of Alzheimer's and other neurodegenerative diseases? *Free Radic. Biol. Med. 33*, 1475−1479.
5. Beckman, K. B., and Ames, B. N. (1998) The free radical theory of aging matures, *Physiol. Rev. 78*, 547−581.
6. Ames, B. N. (2001) DNA damage from micronutrient deficiencies is likely to be a major cause of cancer, *Mutat. Res. 475*, 7−20.
7. Mashima, R., Witting, P. K., and Stocker, R. (2001) Oxidants and antioxidants in atherosclerosis, *Curr. Opin. Lipidol. 12*, 411−418.
8. Cai, H., and Harrison, D. G. (2000) Endothelial dysfunction in cardiovascular diseases: the role of oxidant stress, *Circ. Res. 87*, 840−844.
9. Keaney, J. F., Jr., Larson, M. G., Vasan, R. S., Wilson, P. W., Lipinska, I., Corey, D., Massaro, J. M., Sutherland, P., Vita, J. A., and Benjamin, E. J. (2003) Obesity and systemic oxidative stress: clinical correlates of oxidative stress in the Framingham study, *Arterioscler. Thromb. Vasc. Biol. 23*, 434−439.
10. Porter, N. A., Caldwell, S. E., and Mills, K. A. (1995) Mechanisms of free radical oxidation of unsaturated lipids, *Lipids 30*, 277−290.
11. Roberts, L. J., Salomon, R. G., Morrow, J. D., and Brame, C. J. (1999) New developments in the isoprostane pathway: identification of novel highly reactive gamma-ketoaldehydes (isolevuglandins) and characterization of their protein adducts, *FASEB J. 13*, 1157−1168.
12. Liu, Z., Minkler, P. E., and Sayre, L. M. (2003) Mass spectroscopic characterization of protein modification by 4-hydroxy-2-(E)-nonenal and 4-oxo-2-(E)-nonenal, *Chem. Res. Toxicol. 16*, 901−911.
13. Zhang, W. H., Liu, J., Xu, G., Yuan, Q., and Sayre, L. M. (2003) Model studies on protein side chain modification by 4-oxo-2-nonenal, *Chem. Res. Toxicol. 16*, 512−523.
14. Bolgar, M. S., Yang, C. Y., and Gaskell, S. J. (1996) First direct evidence for lipid/protein conjugation in oxidized human low-density lipoprotein, *J. Biol. Chem. 271*, 27999−28001.
15. Doorn, J. A., and Petersen, D. R. (2002) Covalent modification of amino acid nucleophiles by the lipid peroxidation products 4-hydroxy-2-nonenal and 4-oxo-2-nonenal, *Chem. Res. Toxicol. 15*, 1445−1450.
16. Alderton, A. L., Faustman, C., Liebler, D. C., and Hill, D. W. (2003) Induction of redox instability of bovine myoglobin by adduction with 4-hydroxy-2-nonenal, *Biochem. 42*, 4398−4405.
17. Isom, A. L., Barnes, S., Wilson, L., Kirk, M., Coward, L., and Darley-Usmar, V. (2004) Modification of cytochrome *c* by 4-hydroxy- 2-nonenal: evidence for histidine, lysine, and arginine-aldehyde adducts, *J. Am. Soc. Mass Spectrom. 15*, 1136−1147.
18. Lin, D., Lee, H. G., Liu, Q., Perry, G., Smith, M. A., and Sayre, L. M. (2005) 4-Oxo-2-nonenal is both more neurotoxic and more protein reactive than 4-hydroxy-2-nonenal, *Chem. Res Toxicol. 18*, 1219−1231.
19. West, J. D., Ji, C., Duncan, S. T., Amarnath, V., Schneider, C., Rizzo, C. J., Brash, A. R., and Marnett, L. J. (2004) Induction of apoptosis in colorectal carcinoma cells treated with 4-hydroxy-2-nonenal and structurally related aldehydic products of lipid peroxidation, *Chem. Res. Toxicol. 17*, 453−462.
20. Gard, A. L., Solodushko, V. G., Waeg, G., and Majic, T. (2001) 4-Hydroxynonenal, a lipid peroxidation byproduct of spinal cord injury, is cytotoxic for oligodendrocyte progenitors and inhibits their responsiveness to PDGF, *Microsc. Res Technol. 52*, 709−718.
21. West, J. D., and Marnett, L. J. (2005) Alterations in gene expression induced by the lipid peroxidation product, 4-hydroxy-2-nonenal, *Chem. Res Toxicol. 18*, 1642−1653.
22. Crabb, J. W., O'Neil, J., Miyagi, M., West, K., and Hoff, H. F. (2002) Hydroxynonenal inactivates cathepsin B by forming Michael adducts with active site residues, *Protein Sci. 11*, 831−840.
23. Szweda, L. I., Uchida, K., Tsai, L., and Stadtman, E. R. (1993) Inactivation of glucose-6-phosphate dehydrogenase by 4-hydroxy-2-nonenal. Selective modification of an active-site lysine, *J. Biol. Chem. 268*, 3342−3347.
24. Kuo, C. L., Vaz, A. D., and Coon, M. J. (1997) Metabolic activation of *trans*-4-hydroxy-2-nonenal, a toxic product of membrane lipid peroxidation and inhibitor of P450 cytochromes, *J. Biol. Chem. 272*, 22611−22616.
25. Ando, Y., Brannstrom, T., Uchida, K., Nyhlin, N., Nasman, B., Suhr, O., Yamashita, T., Olsson, T., El, S. M., Uchino, M., and Ando, M. (1998) Histochemical detection of 4-hydroxynonenal protein in Alzheimer amyloid, *J. Neurol. Sci. 156*, 172−176.
26. Mattson, M. P., Fu, W., Waeg, G., and Uchida, K. (1997) 4-Hydroxynonenal, a product of lipid peroxidation, inhibits dephosphorylation of the microtubule-associated protein tau, *Neuroreport 8*, 2275−2281.
27. Carbone, D. L., Doorn, J. A., Kiebler, Z., Ickes, B. R., and Petersen, D. R. (2005) Modification of heat shock protein 90 by 4-hydroxynonenal in a rat model of chronic alcoholic liver disease, *J. Pharmacol. Exp. Ther. 315*, 8−15.
28. Yla-Herttuala, S., Palinski, W., Rosenfeld, M. E., Parthasarathy, S., Carew, T. E., Butler, S., Witztum, J. L., and Steinberg, D. (1989) Evidence for the presence of oxidatively modified low-density lipoprotein in atherosclerotic lesions of rabbit and man, *J. Clin. Invest. 84*, 1086−1095.
29. Uchida, K., Itakura, K., Kawakishi, S., Hiai, H., Toyokuni, S., and Stadtman, E. R. (1995) Characterization of epitopes recognized by 4-hydroxy-2-nonenal specific antibodies, *Arch. Biochem. Biophys. 324*, 241−248.
30. Traverso, N., Menini, S., Cosso, L., Odetti, P., Albano, E., Pronzato, M. A., and Marinari, U. M. (1998) Immunological evidence for increased oxidative stress in diabetic rats, *Diabetologia 41*, 265−270.
31. Roberts, L. J. and Morrow, J. D. (1997) Isoprostanes as markers of lipid peroxidation in atherosclerosis, in *Molecular and Cellular Basis of Inflammation* (Serhan, C. N. and Ward, P. N., Eds.) pp 141−163, Humana Press, Totowa, NJ.
32. Fam, S. S., and Morrow, J. D. (2003) The isoprostanes: unique products of arachidonic Acid oxidation-a review, *Curr. Med. Chem. 10*, 1623−1740.
33. Kadiiska, M. B., Gladen, B. C., Baird, D. D., Germolec, D., Graham, L. B., Parker, C. E., Nyska, A., Wachsman, J. T., Ames, B. N., Basu, S., Brot, N., Fitzgerald, G. A., Floyd, R. A., George, M., Heinecke, J. W., Hatch, G. E., Hensley, K., Lawson, J. A., Marnett, L. J., Morrow, J. D., Murray, D. M., Plastaras, J., Roberts, L. J., Rokach, J., Shigenaga, M. K., Sohal, R. S., Sun, J., Tice, R. R., Van Thiel, D. H., Wellner, D., Walter, P. B., Tomer, K. B., Mason, R. P., and Barrett, J. C. (2005) Biomarkers of oxidative stress study II: Are oxidation products of lipids, proteins, and DNA markers of CCl(4) poisoning? *Free Radic. Biol. Med. 38*, 698−710.
34. Doweiko, J. P. and Nompleggi, D. J. (1991) Role of albumin in human physiology and pathophysiology, *JPEN J. Parenter. Enteral Nutr. 15*, 207−211.
35. Curry, S., Brick, P., and Franks, N. P. (1999) Fatty acid binding to human serum albumin: new insights from crystallographic studies, *Biochim. Biophys. Acta 1441*, 131−140.
36. Anderson, N. L. and Anderson, N. G. (2002) The human plasma proteome: history, character, and diagnostic prospects, *Mol. Cell Proteomics 1*, 845−867.
37. Ding, A., Ojingwa, J. C., McDonagh, A. F., Burlingame, A. L., and Benet, L. Z. (1993) Evidence for covalent binding of acyl glucuronides to serum albumin via an imine mechanism as revealed by tandem mass spectrometry, *Proc. Natl. Acad. Sci. U.S.A. 90*, 3797−3801.
38. Zia-Amirhosseini, P., Ding, A., Burlingame, A. L., McDonagh, A. F., and Benet, L. Z. (1995) Synthesis and mass-spectrometric

characterization of human serum albumins modified by covalent binding of two non-steroidal anti-inflammatory drugs: tolmetin and zomepirac, *Biochem. J. 311* (Pt 2), 431−435.
39. Qiu, Y., Burlingame, A. L., and Benet, L. Z. (1998) Mechanisms for covalent binding of benoxaprofen glucuronide to human serum albumin. Studies by tandem mass spectrometry, *Drug. Metab. Dispos. 26*, 246−256.
40. Day, J. F., Thorpe, S. R., and Baynes, J. W. (1979) Nonenzymatically glucosylated albumin. In vitro preparation and isolation from normal human serum, *J. Biol. Chem. 254*, 595−597.
41. Dockal, M., Carter, D. C., and Ruker, F. (1999) The three recombinant domains of human serum albumin. Structural characterization and ligand binding properties, *J. Biol. Chem. 274*, 29303−29310.
42. Pieper, R., Su, Q., Gatlin, C. L., Huang, S. T., Anderson, N. L., and Steiner, S. (2003) Multi-component immunoaffinity subtraction chromatography: An innovative step towards a comprehensive survey of the human plasma proteome, *Proteomics 3*, 422−432.
43. Hansen, B. T., Jones, J. A., Mason, D. E., and Liebler, D. C. (2001) SALSA: a pattern recognition algorithm to detect electrophile-adducted peptides by automated evaluation of CID spectra in LC-MS-MS analyses, *Anal. Chem. 73*, 1676−1683.
44. Badghisi, H., and Liebler, D. C. (2002) Sequence mapping of epoxide adducts in human hemoglobin with LC-tandem MS and the SALSA algorithm, *Chem. Res. Toxicol. 15*, 799−805.
45. Anderson, W. B., Liebler, D. C., Board, P. G., and Anders, M. W. (2002) Mass spectral characterization of dichloroacetic acid-modified human glutathione transferase zeta, *Chem. Res. Toxicol. 15*, 1387−1397.
46. Lantum, H. B., Liebler, D. C., Board, P. G., and Anders, M. W. (2002) Alkylation and inactivation of human glutathione transferase zeta (hGSTZ1-1) by maleylacetone and fumarylacetone, *Chem. Res. Toxicol. 15*, 707−716.
47. Hansen, B. T., Davey, S. W., Ham, A. J., and Liebler, D. C. (2005) P−Mod: An algorithm and software to map modifications to peptide sequences using tandem MS data, *J. Proteome Res. 4*, 358−368.
48. Mason, D. E. and Liebler, D. C. (2003) Quantitative analysis of modified proteins by LC-MS-MS of peptides labeled with phenyl isocyanate, *J. Proteome Res. 2*, 265−272.
49. Roepstorff, P., and Fohlman, J. (1984) Proposal for a common nomenclature for sequence ions in mass spectra of peptides, *Biomed. Mass Spectrom. 11*, 601.
50. Gerber, S. A., Rush, J., Stemman, O., Kirschner, M. W., and Gygi, S. P. (2003) Absolute quantification of proteins and phosphoproteins from cell lysates by tandem MS, *Proc. Natl. Acad. Sci. U.S.A. 100*, 6940−6945.
51. He, X. M., and Carter, D. C. (1992) Atomic structure and chemistry of human serum albumin, *Nature 358*, 209−215.
52. Zunszain, P. A., Ghuman, J., Komatsu, T., Tsuchida, E., and Curry, S. (2003) Crystal structural analysis of human serum albumin complexed with hemin and fatty acid, *BMC Struct. Biol. 3*, 6.
53. Bhattacharya, A. A., Grune, T., and Curry, S. (2000) Crystallographic analysis reveals common modes of binding of medium and long-chain fatty acids to human serum albumin, *J. Mol. Biol. 303*, 721−732.
54. Petitpas, I., Grune, T., Bhattacharya, A. A., and Curry, S. (2001) Crystal structures of human serum albumin complexed with monounsaturated and polyunsaturated fatty acids, *J. Mol. Biol. 314*, 955−960.
55. Petitpas, I., Petersen, C. E., Ha, C. E., Bhattacharya, A. A., Zunszain, P. A., Ghuman, J., Bhagavan, N. V., and Curry, S. (2003) Structural basis of albumin-thyroxine interactions and familial dysalbuminemic hyperthyroxinemia, *Proc. Natl. Acad. Sci. U.S.A. 100*, 6440−6445.
56. Petitpas, I., Bhattacharya, A. A., Twine, S., East, M., and Curry, S. (2001) Crystal structure analysis of warfarin binding to human serum albumin: anatomy of drug site I, *J. Biol. Chem. 276*, 22804−22809.
57. Li, H., Robertson, A. D., and Jensen, J. H. (2005) Very fast empirical prediction and rationalization of protein pK_a values, *Proteins 61*, 704−721.
58. Dolinsky, T. J., Nielsen, J. E., McCammon, J. A., and Baker, N. A. (2004) PDB2PQR: an automated pipeline for the setup of Poisson−Boltzmann electrostatics calculations, *Nucleic Acids Res. 32*, W665−W667.
59. Sowell, J., Frei, B., and Stevens, J. F. (2004) Vitamin C conjugates of genotoxic lipid peroxidation products: structural characterization and detection in human plasma, *Proc. Natl. Acad. Sci. U.S.A. 101*, 17964−17969.

BI060535Q